Daylight imaging of SSA targets through distributed volume non-Kolmogorov and anisotropic deep turbulence at low elevation angles.

Jeremy P. Bos
NRC Research Associate, Air Force Research Laboratory, Kihei, HI

Abstract

Monte-Carlo simulations featuring Kolmogorov phase screens have long been used in understanding both the effects of atmospheric turbulence on imaging and the performance of turbulence mitigation methods. We have developed a new, high fidelity, non-Kolmogorov phase screen model that allows the orientation of anisotropy to vary arbitrarily. Our model is used to generate simulated video sequences featuring a common satellite-imaging target in low-elevation, daylight imaging scenarios, where these effects are thought to be common. These sequences demonstrate the effects of anisotropic, non-Kolmogorov turbulence, which can be unintuitive. We also briefly examine how these non-traditional features affect the performance of certain post-processing techniques, such as speckle imaging.

1. INTRODUCTION

In Daylight Imaging (DI) of Space Situational Awareness (SSA) targets many objects of interest are often visible from ground-based imaging assets only at low elevation angles. Imaging at low elevation angles is challenging for a number of reasons and even more so during daytime. By far the most challenging aspect is the length of the ground-to-space observation path through the atmosphere. Considering the long path length turbulence is certain to be severe confounding image recovery algorithms. Also challenging is the uncertainty regarding the nature of turbulence along these paths. Recent evidence [1-3] suggests that turbulence along these paths does not obey traditional Kolmogorov, 5/3 power-law fluctuation statistics. This work also suggests that turbulence may be highly anisotropic [3]. The deviation of turbulence from these two norms has been explored in depth analytically by a number of authors and accurate, high fidelity modeling on these effects via simulation is active area of research.

In this work we focus, primarily, on visualizing the effects of non-Kolmogorov and anisotropic turbulence on imaging during DI engagement scenarios using sequences of simulated images. The key development enabling this comparison is a high-fidelity non-Kolmogorov phase screen model. Monte-Carlo phase screen simulations are indispensable in both understanding the effect of turbulence, of any kind, on imaging system and especially in understanding the limits of turbulence mitigation methods such as Adaptive Optics, and image reconstruction methods such as Speckle Imaging (SI) [4] and Multi-Frame Blind Deconvolution (MFBD) [5]. To that point, we briefly examine the effect of anisotropy and changing power law exponent on the ability of SI methods to recover images from multiple turbulence corrupted images. In general, we find that smaller power-law exponent increase image blur though images are subject to relative less tip-tilt distortion. On the other hand, power-law exponents larger than the standard 5/3-value result in increased tip-tilt with less overall blurring. As one might expect, the effect of anisotropy is to preferentially blur images along the direction of the anisotropy. Images recovered using SI-techniques from simulated, turbulence-degraded imagery with these features are surprisingly similar. This similarity implies that turbulence strength and image frame SNR is more critical than the specific nature of the turbulence distortion, i.e. power-law exponent or anisotropy.

2. BACKGROUND

Monte-Carlo simulation involving Kolmogorov phase screens have been use for many years and are a standard tool in atmospheric optics. Though other methods exist [6,7] most commercially available atmospheric optics products , such as WaveProp, make use of phase screens generated using FFT-based techniques. FFT-based methods begin with a matrix, W_n, of complex circular Gaussian random numbers with the same number of samples as the desired phase screen. The inverse Fourier transform of the product between an appropriately sampled covariance matrix,

$$\phi_n = \mathcal{F}^{-1}\{W_n * (\Phi(\kappa))^{-1/2}\}^{-1} \quad (1)$$

results in two independent phase screens with the correct spatial statistics. In Eq. (1), $\Phi(\kappa)$, is the Power Spectral Density (PSD) model of the turbulence fluctuation statistics.

Report Documentation Page		*Form Approved* *OMB No. 0704-0188*

1. REPORT DATE **SEP 2014**	2. REPORT TYPE	3. DATES COVERED **00-00-2014 to 00-00-2014**

4. TITLE AND SUBTITLE	5a. CONTRACT NUMBER
Daylight Imaging of SSA Targets Through Dstributed Volume non-Kolmogorov and Anisotropic Deep Turbulence at Low Elevation Angles	5b. GRANT NUMBER
	5c. PROGRAM ELEMENT NUMBER
6. AUTHOR(S)	5d. PROJECT NUMBER
	5e. TASK NUMBER
	5f. WORK UNIT NUMBER

7. PERFORMING ORGANIZATION NAME(S) AND ADDRESS(ES) **Air Force Research Laboratory,Kihei,HI,96753**	8. PERFORMING ORGANIZATION REPORT NUMBER

9. SPONSORING/MONITORING AGENCY NAME(S) AND ADDRESS(ES)	10. SPONSOR/MONITOR'S ACRONYM(S)
	11. SPONSOR/MONITOR'S REPORT NUMBER(S)

12. DISTRIBUTION/AVAILABILITY STATEMENT

Approved for public release; distribution unlimited

13. SUPPLEMENTARY NOTES

In the Advanced Maui Optical and Space Surveillance Technologies (AMOS) Conference, 9-12 Sep 2014, Maui, HI.

14. ABSTRACT

Monte-Carlo simulations featuring Kolmogorov phase screens have long been used in understanding both the effects of atmospheric turbulence on imaging and the performance of turbulence mitigation methods. We have developed a new, high fidelity, non-Kolmogorov phase screen model that allows the orientation of anisotropy to vary arbitrarily. Our model is used to generate simulated video sequences featuring a common satellite-imaging target in lowelevation daylight imaging scenarios, where these effects are thought to be common. These sequences demonstrate the effects of anisotropic, non-Kolmogorov turbulence, which can be unintuitive. We also briefly examine how these non-traditional features affect the performance of certain post-processing techniques, such as speckle imaging.

15. SUBJECT TERMS

16. SECURITY CLASSIFICATION OF:			17. LIMITATION OF ABSTRACT	18. NUMBER OF PAGES	19a. NAME OF RESPONSIBLE PERSON
a. REPORT **unclassified**	b. ABSTRACT **unclassified**	c. THIS PAGE **unclassified**	**Same as Report (SAR)**	**8**	

A recognized weakness of this method is an under sampling at low spatial frequencies. This weakness is especially worrisome considering that most of the turbulence energy in a volume of atmosphere is found in the outer scales and therefore also the lower spatial frequencies. Lane [8] originally suggested what has become known as the "sub-harmonic" compensation method. Lane's method samples the lowest spatial frequency region of the PSD model enhancing the accuracy of the model. Frelich [9], and later Schmidt [10], both describe an implementation of the sub-harmonic technique including 3 sub-harmonics, though generalizing the technique to additional samples is a trivial task.

Apart from some early, generalized, work by Martin [11] and Coles [12] there has been little attention paid to the non-Kolmgorov power-law phase screen in the area of optical wave propagation in the atmosphere. Most work in the area, up to now, has focused on the development of analytical models. The first non-Kolmogorov phase screen model was reported by Gudimetla [13]. Recently, Roggemann [14], and separately Bos [15] have presented work on simulations involving non-Kolmogorov phase screens. In both cases, the user may select the power law exponent as well as inner and outer scale. The latter are modeled using a generalized form of the analytical Tatarskii spectrum in terms of radial wavenumber κ and power-law exponent α is

$$\Phi(\kappa) = A(\alpha)\beta \frac{\exp\left(-\kappa^2 / \kappa_m^2\right)}{\left(\kappa^2 + \kappa_0^2\right)^{\alpha/2}} \tag{2}$$

In Eq.(2), $A(\alpha) = \frac{1}{4\pi^2} \Gamma(\alpha - 1) cos\left(\frac{\alpha\pi}{2}\right)$ is a parameter that maintains consistency between structure function

and power spectrum models of index of refraction fluctuations. The parameter β is a strength parameter equivalent to C_n^2 when $\alpha = 11/3$. The variables $\kappa_0 = 2\pi / L_0$ and $\kappa_m = c(\alpha)/l_0$ parameters for the outer-scale, L_0, and inner-scale, l_0, respectively with $c(\alpha)$ being the inertial-dissipative consistency parameter [18]. Both Bos [15] and Roggemann [14] use include Lane's sub-harmonic compensation method. The model used here adds the ability to vary both the degree and direction of anisotropy. Anisotropy is introduced following the model described by Wheelon [16] and later Gudimetla [17] via affine transform of the spatial coordinates.

$$\vec{f} = (f_x^2 + f_y^2)^{1/2} = (ab)^{1/2}\left(\frac{1}{a}f_x^2 + \frac{1}{b}f_y^2\right)^{1/2} \tag{3}$$

Varying the direction of the anisotropy is enabled via a second affine transform of the covariance-sampling matrix.

$$f_{x'} = f_x \cos\theta + f_y \sin\theta$$
$$f_{y'} = -f_x \sin\theta + f_y \cos\theta \tag{4}$$

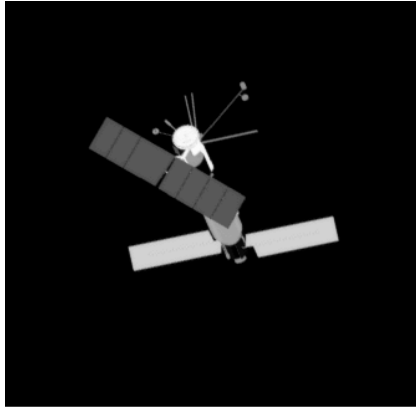### 3. GENERATED SIMULATED IMAGERY USING PHASE SCREEN MODEL

Fig. 1: Pristine SEASAT Image

Phase screens generated using the technique described above were used to generate simulated imagery of a common "SEASAT" (Fig.1) SSA target corrupted by atmospheric turbulence. Simulation was carried out by placing a single phase screen across D=3.5m imaging aperture using the technique described by Roggemann [4]. When not specified, turbulence strength was fixed at $D/r_0 = 10$. Taking a new draw of the circular complex Gaussian random matrix, W_n, creates new, independent phase screens and subsequently, new, statistically independent images. By placing these images in sequence we can create video sequences that either demonstrate the range of fluctuations under static conditions or visualize the effect of a changing variable. Keystones for several of these video sequences are shown in the next section.

4. VIDEO SEQUENCES: EFFECT OF VARIED D/ r_0 FOR VARIOUS POWER LAW EXPONENTS
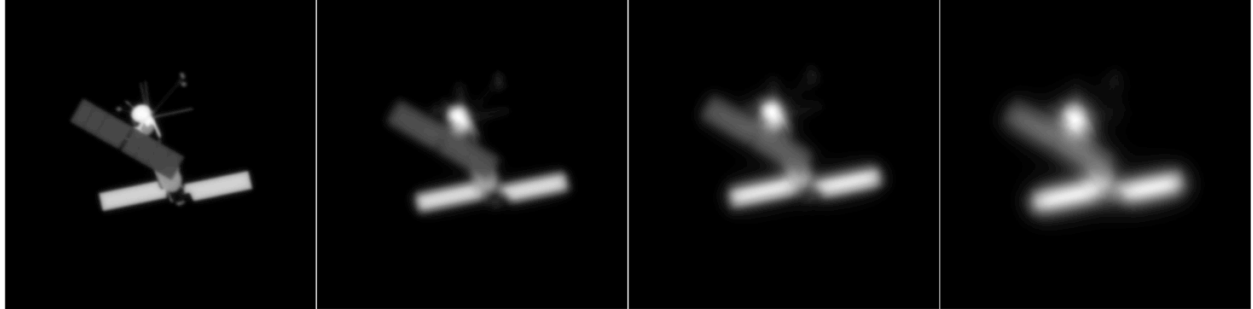
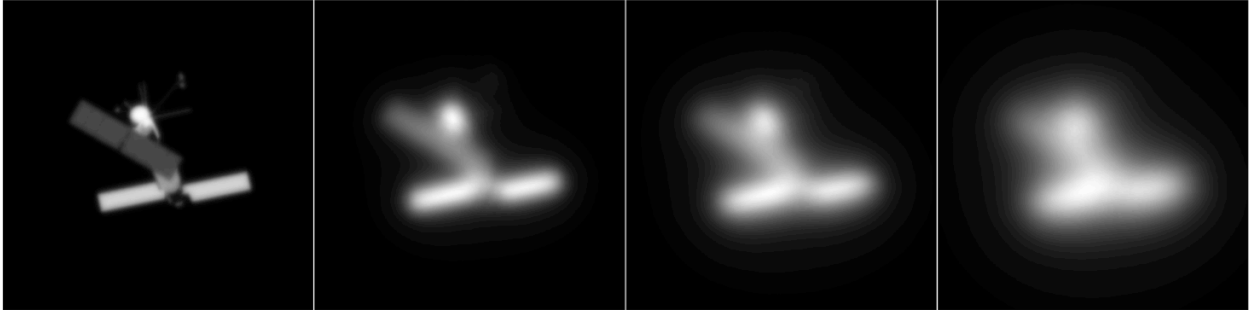

Fig. 2: D/r0 = 10 to 40, α = 11/3 (Kolmogorov turbulence)

Fig. 3: D/r0 = 10 to 40, α = 3.1 (non-Kolmogorov turbulence, near lower bound)
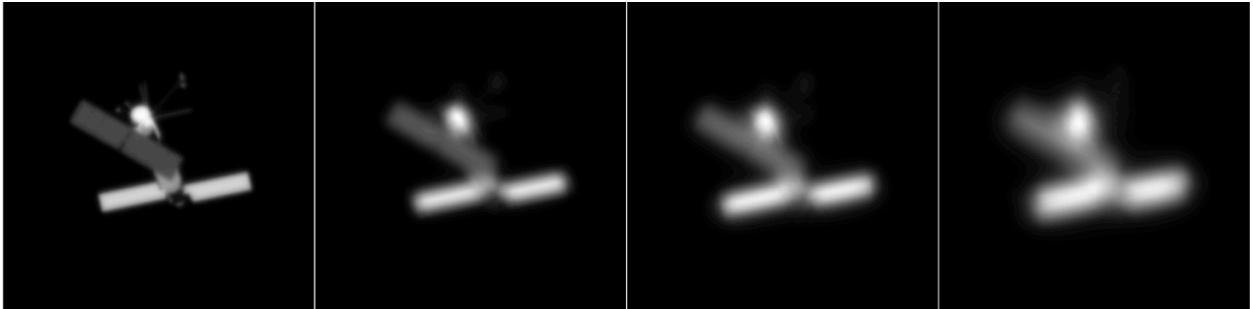

Fig. 4: D/r0 = 10 to 40, α = 3.8 (non-Kolmogorov, near upper bound)

Fig.2 show several frames from a video sequence where the turbulence strength, in terms of D/r_0 is varied between 10 and 40 while the power-law exponent is fixed at α = 11/3, or typical Kolmogorov turbulence. The full video sequence begins with a relatively unperturbed image that gradually becomes more distorted and also shifts randomly around the image frame, both characteristics of turbulence-induced imaging distortions. Fig.3 is similar to Fig.2 but the phase screen power-law exponent has been changed to α = 3.1. We observe that the tip-tilt/random motion effects are nearly absent in this sequence while relative blurring is more severe. Finally, in Fig.4 the power-law exponent has been changed to α = 3.8. In Fig.4 both blurring and tip-tilt distortions are more severe, the latter being more pronounced that in the other two cases. We note briefly here that the structure function definition of turbulence is limited to a range of 3 < α < 5. However, the wave structure function, and all parameters derived therefrom are

limited to the range $3 < \alpha < 4$. Our phase screen model uses the Fried parameter to set turbulence strength. Of course, the Fried parameter is defined as the point where the Kolmogorov wave structure function is equal to 6.88.

Fig. 5: Degree of anisotropy varied from 0 to 3 at D/r0 = 20

We now focus on the topic of anisotropic turbulence, the presence of which is thought to be commonplace in the upper atmosphere. Accordingly, any low-elevation angle, earth-to-space imaging path will traverse long section sections of the upper atmosphere and, therefore, likely subject to anisotropic turbulence. In Fig.5 we demonstrate the effect degree of anisotropy, ε, from 0 to 3. In our model this variation results in anisotropy along the vertical direction. As expected, in Fig.5 we observe a very clear increase in horizontal blurring as the anisotropy factor is increased.

5. SIMPLE SI IMAGE RESTORATION

In this section, we compare images reconstructed using a research SI processing technique from sequences of turbulence imagery. Our SI processing technique uses no SNR weighting or other optimizations and is identical to the bispectrum method described in [19]. As in that work, 5 sub-planes of the bispectrum are averaged to determine the image phase at each spatial frequency. Our objective here is to determine if changes in power-law or anisotropy may adversely affect reconstruction quality. In all cases, all parameters are fixed and 100 input frames are used for each reconstruction. To begin, additive and photon-counting noise effects are not included.
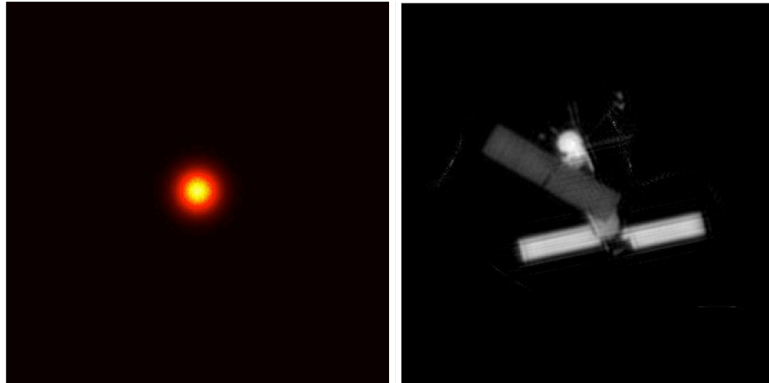

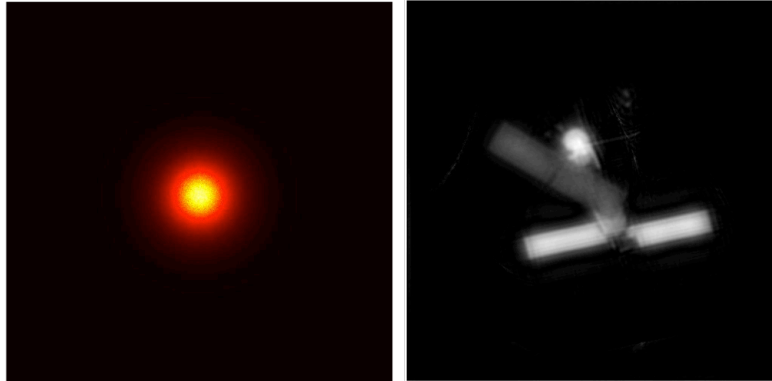**Fig. 6: 100-frame long-exposure PSF at α=3.66 (11/3) (left). 100 frame SI-reconstruction at D/r0 = 10 (right)**

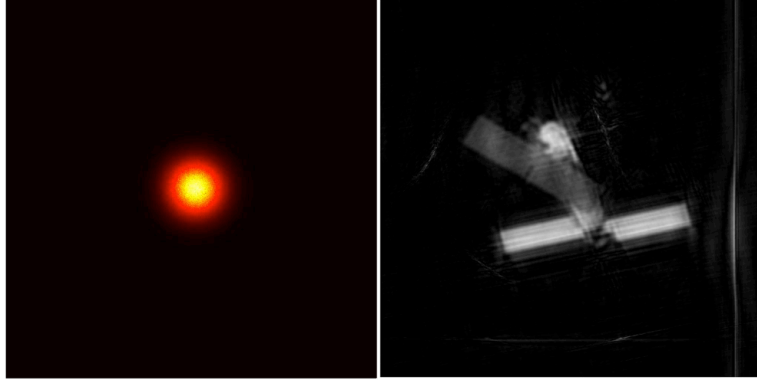**Fig. 7: 100-frame long-exposure PSF at α=3.1 (left). 100 frame SI-reconstruction at D/r0 = 10 (right)**

Fig. 8: 100-frame long-exposure PSF at α=3.8 (left). 100 frame SI-reconstruction at D/r0 = 10 (right)

We consider the isotropic, Kolmogorov results shown in Fig.6 (right) as the baseline for comparison in this section. To that point, we observe that the PSF in both Fig.7 and Fig.8 are wider than the baseline. Likewise, in Fig.8 the PSF is wider and, by examining the video sequence a considerable larger bulk tip-tilt component is observed. Comparing reconstruction results (right) in each figure we observe, in general, little difference in reconstruction quality between images. That is to say, there are no features in the baseline that cannot be observed in the other images. On a finer scale, both non-Kolmogorov cases result in a degradation of image quality. In the "low" power-law case (α = 3.1) the image is blurred compared to the baseline. It is possible that additional tuning of the noise parameter in the pseudo-Weiner inverse filter may further improve this image. In contrast, the "high" power law case (α = 3.8) contains imaging artifacts common in SI-reconstructions where the object drifts beyond the image frame. It is often possible to correct these artifacts so, while undesirable, they don't rule out the use of speckle imaging here.
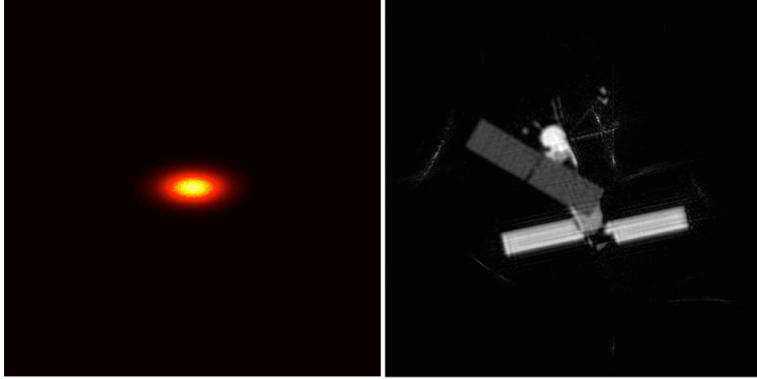

Fig. 9: 100-frame, long-exposure PSF (left) and SI-reconstruction (right) for non-Kolmogorov turbulence with anisotropy factor ε=2.
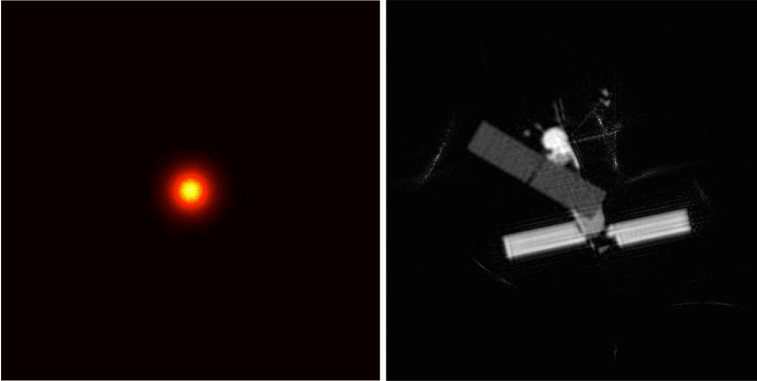

Fig. 10: 100-frame, long-exposure PSF (left) and SI-reconstruction (right) for non-Kolmogorov turbulence with anisotropy factor ε=2. The direction of anisotropy varies continuously from 0 to 180 degrees.

In Fig.9 we show an example turbulence-degraded image, PSF, and the 100-frame reconstruction for turbulence with an anisotropy factor of $\varepsilon = 2$. In contrast to Fig.5, atmospheric distortions are more severe in the horizontal, rather than vertical direction in Fig.9. Relative turbulence strength is kept fixed at D/r0 = 10. The reconstruction in Fig.9 is subjectively equivalent to, if not slightly better than, the baseline reconstruction in Fig.5. This result is expected considering the use of the affine transform in our phase screen model. Consequently, when anisotropy is increased along one axis it is decreased in the other effectively increasing coherence. Thus, we might expect improved resolution in the vertical direction relative to the isotropic case. In Fig.9 it is difficult to conclude one way or the other if such improvement is present. Considering the cursory nature of this exercise we will leave such exploration for another time.

In Fig.10, like Fig.9, input images are blurred by anisotropic turbulence with a factor of $\varepsilon=2$. However, rather than being fixed along one axis, the orientation of the anisotropy changes. Anisoptropy is directed along the horizontal axis at the start of the sequence, as the sequence progresses the orientation changes; falling along the vertical axis at the midpoint and returning to the horizontal axis again by the last frame. By way of implementation the angle of anisotropy varies from 0 to 180 degrees. Assuming fixed anisotropy one can approximate this scenario as one where the orientation of the satellite varies relative to the anisotropy over the course an observation pass. Examining the reconstructed frame in Fig.10 we observe both more contrast than Fig.5 or Fig.9 but also more prominent artifacts. We speculate that additional tuning of the noise parameter may ameliorate the differences producing an imaging with both improved contrast and/or detail and less prominent processing artifacts. Finally, we observe that the PSF in Fig.10 (left) is no smaller than the isotropic, Kolmogorov case.
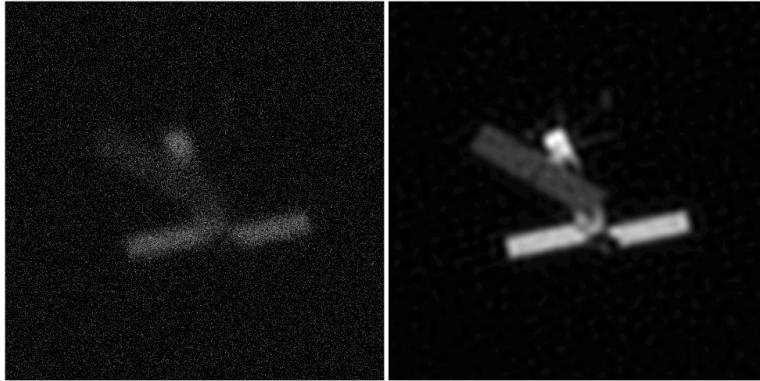

Fig. 11:Sample image frame (left) and SI-reconstruction (right) in including Poisson and Gaussian noise for isotropic, Kolmogorov turbulence.
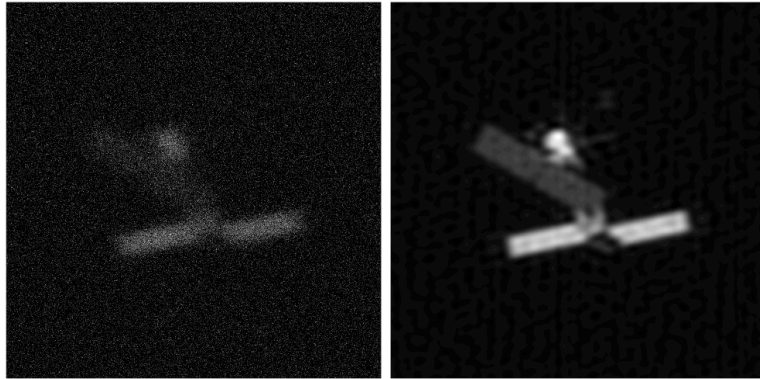

Fig. 12: Sample image frame (left) and SI-reconstruction (right) in including Poisson and Gaussian noise for anisotropic turbulence with Kolmogorov power-law exponent.

Fig. 11 and Fig. 12 repeat the cases in Fig.5 and Fig.10 but include both additive Gaussian noise and Poisson noise associated with photo-detection events. Additive noise in this case models both the background noise and read-noise associated with the detector. Noise in this case was zero mean with a deviation of $\sigma_n=100$. Poisson noise was modeled by using normalizing intensity to unit energy and scaling by K=5,000,000 photo-events, $D/r_0 =10$ in all cases. Images were zero thresholded to approximate the decrease in SNR associated with increased background illumination during DI scenarios. In Fig.11 and Fig.12 the image on the left is an example input image and the right

the SI output. Though a point result, the anisotropic results in Fig.12 are subjectively better than the isotropic, Kolmogorov case in Fig.11. Again, this result is not unexpected, as anisotropy results in increased coherence in one direction. Fig.12 also includes faint artifacts hinting that severe anisotropy may pose problems for speckle imaging. In Fig.13 and 14, example frames and point reconstructions are shown for power-laws of α=3.1 and 3.8 respectively. The reconstruction in Fig.13 is degraded compared to Fig.11. The results here make sense if we compare the long-exposure PSF in Fig.6 and 7 and assume that the effect of the smaller power law is in effect the same as an increase in turbulence strength. In contrast, we judge Fig.11 and Fig.14 to be roughly equivalent. Though the PSF in Fig.8 is also wider than Kolmogorov case, as we discussed previously, the majority of the distortion here is from tip-tilt. The bispectrum is immune to in-frame tip-tilt distortion, and so, does not degrade image quality.

6. CONCLUSIONS

We have developed a new and novel method of producing turbulence phase screens with several features important to modeling DI engagements. We have used this model to produce video sequences featuring both non-Kolmogorov turbulence and turbulence with varied degree and direction of anisotropy. The improved modeling capability presented here will allow for the simulation of complex engagement scenarios where parameters such as turbulence strength, power-law, degree and direction of anisotropy all very simultaneously. Preliminary results, shown here, indicate that basic SI techniques remain effective when turbulence is non-Kolmogorov and for reasonable levels of anisotropy even in the presence of Poisson and additive noise associated with increased background illumination. The one possible exception being scenarios where high power-law exponents increase turbulence-induced in-frame jitter. Optimistically, this jitter could be corrected using a Fast-Steering Mirror or by dropping frames where the object impinges on the edge of the frame.
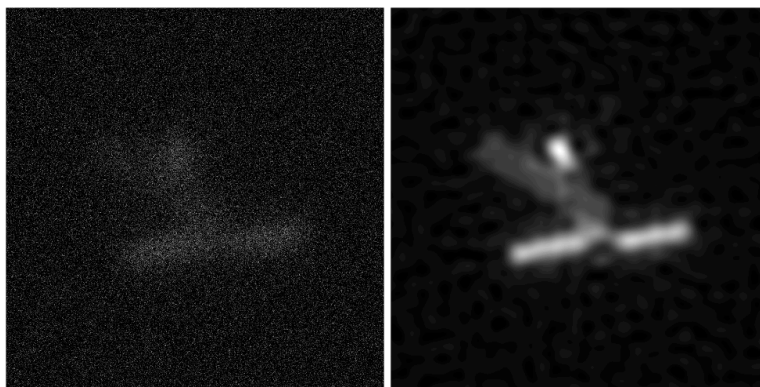

Fig. 13: Sample image frame (left) and SI-reconstruction (right) in including Poisson noise for anisotropic turbulence with non-Kolmogorov power-law exponent of α=3.1 .
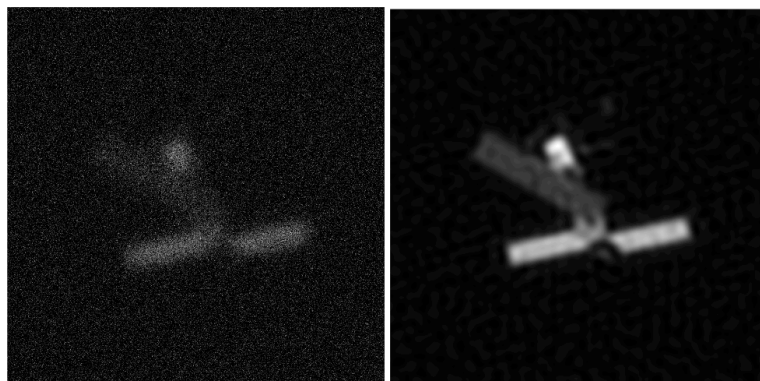

Fig. 14: Sample image frame (left) and SI-reconstruction (right) in including Poisson noise for anisotropic turbulence with non-Kolmogorov power-law exponent of α=3.8.

7. <u>References</u>

[1] J.T. Beyer, M.C. Roggemann, L.J. Otten, T.J. Schulz, T.C. Havens, and W.W. Brown, "Experimental estimation of the spatial statistics of turbulence-induced index of refraction fluctuations in the upper atmosphere," Appl. Opt. **42**, 908–921 (2003).

[2] F.Dalaudier, C. Sidi, M.Crochet, and J.Vernin, "Direct evidence of sheets in the atmospheric temperature field," Journal of the Atmospheric Sciences **51**(2), 237–248 (1994).

[3] M.S. Belen'kii, S. J. Karis, C.L. Osmon, J.M. Brown II, and R.Q. Fugate, "Experimental evidence of the effects of non-kolmogorov turbulence and anisotropy of turbulence," Proc. SPIE 3749, 50–51 (1999).

[4] Roggemann, M. C., B.M. Wels, *Imaging through turbulence*, CRC press, 1996.

[5] Schulz, Timothy J. "Multiframe blind deconvolution of astronomical images." JOSA A 10.5 (1993): 1064-1073.

[6] R. J. Noll, "Zernike polynomials and atmospheric turbulence," J. Opt. Soc. Am. **66**, 207–211 (1976).

[7] M. Charnotskii, "Sparse spectrum model for a turbulent phase," J. Opt. Soc. Am. A **30**, 479–488 (2013).

[8] R. Lane, A. Glindemann, J. Dainty, et al., "Simulation of a kolmogorov phase screen," Waves in random media **2**(3), 209–224 (1992).

[9] R. Frehlich, "Simulation of laser propagation in a turbulent atmosphere," Appl. Opt. **39**, 393–397 (2000).

[10] J. D. Schmidt, *Numerical simulation of optical wave propagation with examples in MATLAB*, SPIE Press (2010).

[11] J. Martin and S. M. Flatte, "Intensity images and statistics from numerical simulation of wave propagation in 3-d random media," Applied Optics **27**(11), 2111–2126 (1988).

[12] W. A. Coles, J. Filice, R. Frehlich, and M. Yadlowsky, "Simulation of wave propagation in three-dimensional random media," Applied optics **34**(12), 2089–2101 (1995).

[13] V. S. R. Gudimetla, R. B. Holmes, T. C. Farrell, and J. Lucas, "Phase screen simulations of laser propagation through non-kolmogorov atmospheric turbulence," Proc. SPIE 8038, 803808–803808–12 (2011).

[14] M. C. Roggemann, "Simulating non-kolomogorov phase screens," in Imaging and Applied Optics 2014, Imaging and Applied Optics 2014 , PM4E.1, Optical Society of America (2014).

[15] J. P. Bos and V. S. Gudimetla, "Simulation of long-path horizontal propagation through a three-layer non-kolmogorov atmosphere model," in Imaging and Applied Optics 2014, Imaging and Applied Optics 2014 , PM3E.5, Optical Society of America (2014).

[16] A. D. Wheelon, *Electromagnetic scintillation*, Cambridge University Press (2003).

[17] V. S. R. Gudimetla, R. B. Holmes, C. Smith, and G. Needham, "Analytical expressions for the log-amplitude correlation function of a plane wave through anisotropic atmospheric refractive turbulence," J. Opt. Soc. Am. A **29**, 832–841 (2012).

[18] I. Toselli, L. C. Andrews, R. L. Phillips, and V. Ferrero, "Angle of arrival fluctuations for free space laser beam propagation through non kolmogorov turbulence," Proc. SPIE **6551**, 65510E (2007)

[19] J.P. Bos and M. C. Roggemann, "Technique for simulating anisoplanatic image formation over long horizontal paths," Optical Engineering **51**(10), 101704–1–101704–8 (2012).